Growth, Percolation, and Correlations in Disordered Fiber Networks

N. Provatas,[1] M. Haataja,[1,2] E. Seppälä,[3] S. Majaniemi,[1] J. Åström,[5] M. Alava,[3,4] and T. Ala-Nissila[1,2,6,7]

This paper studies growth, percolation, and correlations in disordered fiber networks. We start by introducing a 2D continuum deposition model with effective fiber–fiber interactions represented by a parameter p which controls the degree of clustering. For $p = 1$ the deposited network is uniformly random, while for $p = 0$ only a single connected cluster can grow. For $p = 0$ we first derive the growth law for the average size of the cluster as well as a formula for its mass density profile. For $p > 0$ we carry out extensive simulations on fibers, and also needles and disks, to study the dependence of the percolation threshold on p. We also derive a mean-field theory for the threshold near $p = 0$ and $p = 1$ and find good qualitative agreement with the simulations. The fiber networks produced by the model display nontrivial density correlations for $p < 1$. We study these by deriving an approximate expression for the pair distribution function of the model that reduces to the exactly known case of a uniformly random network. We also show that the two-point mass density correlation function of the model has a nontrivial form, and discuss our results in view of recent experimental data on mss density correlations in paper sheets.

KEY WORDS: Continuum percolation; deposition models; fiber networks; spatial correlations.

[1] Research Institute for Theoretical Physics, P.O. Box 9 (Siltavuorenpenger 20 C), FIN-00014 University of Helsinki, Helsinki, Finland.
[2] Laboratory of Physics, Tampere University of Technology, FIN-3101 Tampere, Finland.
[3] Laboratory of Physics, Helsinki University of Technology, Otakaari 1 M, FIN-02150 Espoo, Finland.
[4] Department of Physics and Astronomy, Michigan State University, East Lansing, Michigan 48824-1116.
[5] Department of Physics, University of Jyväskylä, P.O. Box 35, FIN-40351 Jyväskylä, Finland.
[6] Department of Physics, Brown University, Providence, Rhode Island 02912.
[7] To whom correspondence should be addressed; e-mail address: ala@phcu.helsinki.fi.

1. INTRODUCTION

There are many phenomena in nature that can be viewed as deposition processes where various transport mechanisms bring particles to a surface. These include many different examples, such as deposition of colloidal, polymer, and giber particles.[1-7] Many deposition phenomena involve particles whose size is large compared to the their mutual interaction range, and so the main deposition mechanism is due to particle exclusion. Among the most studied in this class are the random and cooperative sequential adsorption models.[1,2] There particles are deposited on a surface and either stick or are rejected accoding to certain exclusion rules, with a maximum coverage (the "jamming limit") less than unity. These types of models should be contrasted to the case of multilayer surface groth,[1,6,7] where the main focus is in the asymptotic behavior of the growing surface in the continuum limit.[8]

A particularly interesting and challenging example involving particle deposition can occur in the case of colloidal suspensions. For some such systems the interparticle repulsion is strong enough to prevent multilayer growth.[3] However, the existence of dispersion forces can cause the particles to flocculate, or aggregate, and to precipitate out of the suspension.[7,9] For larger particles or clusters of particles gravity often induces sedimentation out of the suspension. Experiments reveal that sedimentation produces nontrivial spatial structures.[10] A full microscopic treatment of sedimentation is a formidable task, however.[11]

An interesting practical deposition process is the formation of laboratory paper. Paper is manifactured from a colloidal suspension, out of which fibers filtrate onto a wire mesh, leaving behind a fiber network.[4] Recent experimental measurements of mass density correlations in laboratory-made paper sheets reveal[12] that the spatial distribution of fibers may not be uniformly random. In particular, for low-mass-density paper nontrivial power-law-type correlations of the local mass density are found that may extend an order of magnitude beyond the fiber length. This implies that there are nontrivial interactions present during the formation process. A microscopic understanding of this is currently missing. Because of this, phenomenological deposition models may be useful in studying how various effective interactions influence the mass density distribution of the deposit.[12]

In addition to their practical applications, random deposition models have been the topic of intense study in their own right. In particular, they have been extensively studied in the context of continuum percolation theory.[13-27] These models have included both uniformly random networks of various objects as well as some that include hard- and soft-core interactions

between the constituent particles. The quantity of central importance in these studies is the percolation threshold or critical particle density, which for permeable objects can be related to the excluded volume of the particles.[19] This quantity depends on the geometrical shape of the deposited particles as well as on interactions between them in a nontrivial way.

Motivated by processes involving deposition, sedimentation, and the theory of continuum percolation, we introduce and present a detailed study of the properties of a simple 2D deposition model in this work. In the model the tendency of the deposited particles to form clusters is taken into account through a parameter $0 \leqslant p \leqslant 1$. For $p = 1$ the deposition process is uniformly random, while for $p = 0$ only a single connected cluster grows from an initial seed fiber. We study the growth dynamics, percolation thresholds, and spatial correlations of the structures formed by the model in detail, using both analytic and numerical methods. In particular, we discuss our results in view of the experimentally observed mass density correlations in paper sheets.[12]

The outline of this paper is as follows. We first introduce our deposition model in Section 2. In Section 3 we examine the growth properties of single clusters in the limit $p = 0$. After this we present both numerical and analytic results for the percolation threshold of fibers and various other objects as a function of p. Section 5 deals with the theory of spatial correlations in networks formd by the model; in particular, we concentrate on the form of the pair distribution and two-point mass density correlation functions. Finally, Section 6 contains our summary and conclusions.

2. THE MODEL

The model studied in this paper, called the "flocculation model," is in part motivated by the tendency of fibers to stick adhesively during paper-making.[4, 8] The model is a continuum deposition model defined on a 2D surface. Spatially extended objects, such as disks and fibers with a finite area, or widthless needless are individually deposited by the following rules. First, both the orientation of the object as well as its spatial coordinates are chosen from a uniformly random distribution. If a deposited object lands on another object already on the surface, the attempt is always accepted. However, if it lands on empty space, the attempt is accepted only with a given probability p. Thus, the parameters that characterize the model are the acceptance probability p, the dimensions of the deposited objects, the linear dimension L of the surface, and the number of deposited

[8] This model was suggested to us by Jussi Timonen and originally introduced in ref. 28 and ref. 29.

objects kept, N (i.e., the number of accepted attempts). In this work the deposited objects are mostly fibers (rectangles of finite area and varying dimensions); however, in Section 4 we also consider needles (widthless sticks) as well as disks.

In the limit $p = 1$ the model reduces to the extensively studied case of a uniformly random network.[4, 13–17, 23, 27] However, for $p < 1$ it is clear that there are effective interactions betwee the particles that tend to enhance cluster formation within the deposit. In particular, for the extreme case of $p = 0$ only particles that always touch each other are accepted, and a single, connected cluster grows (assuming there is an initial seed particle). We expect all the properties of the growing network, including its percolation threshold and spatial mass density correlations, to depend on p in a non-trivial way. We note that the definition of the model here is different from the extensively studied clss of random sequential adsorption models, where particle overlap is *not* allowed.[1]

3. GROWTH OF INDIVIDUAL FIBER CLUSTERS

First we examine the deposition of fibers in the limit $p = 0$ of the model,[29] where only one connected fiber cluster grows from an initially deposited seed fiber. Figure 1 shows a typical cluster for $N = 2000$ fibers of length $\lambda = 1$ and width $\omega = 1/4$. An individual cluster has an irregular, ragged shape, for which an average radius $R_i(N)$ can be defined. When a statistical average is taken over all possible clusters of size N the average cluster is spherically symmetric and one can define an average radius $R(N) = \langle R_i(N) \rangle$ for which an expression can be obtained by the following argument. Consider the more general d-dimensional case of a cluster of $N \gg 1$ identical fibers of linear dimension a where additional ΔN fibers are
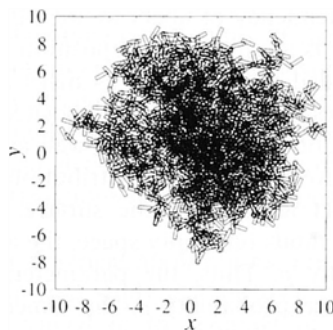

Fig. 1.   A snapshot of a single growing fiber cluster for $N = 2000$ fibers of length $\lambda = 1$ and width $\omega = 1/4$.

deposited. Its radius grows by ΔR and area by ΔA. The change in the cluster area is $\Delta A \propto a^d (R^{d-1}/R^d)\, \Delta N \propto R^{d-1}\, \Delta R$, which in the continuum limit given

$$R(N) = BN^{1/(d+1)} \tag{1}$$

where B is a constant proportional to a. In particular, for the two-dimensional case this means that the average size of the cluster grows as $N^{1/3}$, as already shown in refs. 28 and 29.

The radial mass density of the average fiber cluster was also examined in refs. 28 and 29. For $N \gg 1$ (typically $N > 500$) required for the scaling relation (1) it was shown numerically in ref. 29 that all the density profiles scale onto one curve. The approximate form of this profile can be obtained by the following argument, following ref. 28. Let $\rho(r, N)$ denote the local mass density in a fiber cluster of N fibers, and K the constant flux of mass per unit area onto the luster of radius $R(N)$. Assuming that the rate of change of ρ is proportional to the flux and inversely proportional to the area of the cluster within the cluster radius, then we can write the equation for ρ as

$$\frac{\partial \rho(r, N)}{\partial N} = \frac{K}{\pi R^2(N)}, \qquad 0 < r < R(N) \tag{2}$$

For $r > R(N)$, we assume the flux to be zero. Using Eqs. (1) and (2), we obtain

$$\rho(r, N) = \frac{3K}{\pi B^3} R(N) \left(1 - \frac{r}{R(N)} \right) \tag{3}$$

Equation (3) is in good agreement with the numerically obtained density profiles in ref. 29.

However, as already noted in ref. 29, at the edge of the average cluster there is a systematic deviation from the linear decrease of the density profile to a slower decay law. This indicates that the edge of the cluster is rough, and that the roughness also grows as a function of N. This can be characterized by calculating the average width from the definition

$$w(N) = [\langle (R_i(N) - R(N))^2 \rangle]^{1/2} \tag{4}$$

Since the nonlinear edge of the density profile scales, too, we expect that $w(N)/R(N) = \text{const}$ for $N \gg 1$. We have numerically simulated $w(N)$ in 2D and indeed find that it grows proportional to $N^{1/3}$.

4. PERCOLATION PROPERTIES OF THE MODEL

When enough fibers are deposited in a finite system its edges become connected and percolation takes place in the model. The properties of the corresponding *continuum percolation transition* are of particular interest.[19,30] For the case of single cluster growth the growth law of Eq. (1) implies that $N \propto R^3$. Thus, within a finite system L a single cluster spans the system only when $R \approx L$, which means that the density of fibers $\eta = N/L^2 \propto L$, i.e., it increases with the system size. This means that the critical density η_c for prcolation becomes infinite for $p = 0$. However, for $p > 0$ there is a finite probability of nucleation of multiple clusters and thus η_c should be finite. Indeed, continuum percolation of 2D rectangles,[13,16] disks,[13,14,16,18,19,21,22,26] and needles,[13,15-17,23,28] among other geometric objects, has been extensively studied, and the corresponding critical densities determined numerically. In this section we present results of numrical and analytic calculations of the percolation properties of our model for $0 < p \leqslant 1$ and compare the limit $p = 1$ with the existing studies.

4.1. Numerical Results

We first present results of extensive numrical simulations of the critical densities of percolation $\eta_c(p)$ as a function of p for the three different geometric objects: needles of length λ, fibers (rectangles) of length λ and width ω ($\lambda > \omega$), and disks of radius r_d. The details of the method we have used are as follows. First, each system contains an inner box of length L and an outer box $L + L'$, with free boundary conditions. It is important in the present case to choose L' to be large enough so that the average density across the system is constant within the inner box.[9] The centers of the objects are distributed within the outer box. However, only objects partially or completely within the inner box are allowed to belong to the connected clusters. To keep track of the clusters, we employ a simple labeling technique.[31]

In analyzing the data, we distinguish two different types of percolation processes. In the one-sided case any two opposite edges of the inner box percolate, while in the two-sided case all four edges must become connected. In our final analysis only one-sided percolation data were used.[10]

---

[9] We have checked the density profiles explicitly as a function of p and find that near $p = 1$, L' need not be larger than the largest object dimension. However, for the smallest values of p studied here we find that L' must be about five times larger.

[10] According to ref. 17, if the critical number density is taken to be the average of the values obtained for the one- and two-sided cases, the finite-size correction should approximately cancel out. We checked this for needles, but found it not to be true.

We obtained the critical density η_c by the following procedure. We deposited a fixed number of objects N for a given system size L and checked for percolation. By repeating this 100–1000 times, we obtained the spanning probability, i.e., the fraction of percolating ensembles. Repeating this procedure for various values of N, we obtained the whole curve of spanning probabilities for each system size L as a function of the density $\eta = N/L^2$. The point where two such curves for any different system sizes intersect gives an approximate value for η_c. We obtained these points by fitting the curves to error functions. The estimates thus obtained were extrapolated and the final values of η_c obtained using the standard Monte Carlo renormalization group method,[32,21] with the smallest system studied being the reference system. For completeness we have also evaluated the correlation length exponent v for our model from the MCRG procedure. We note that it is expected to have the well-known value of 4/3 as in lattice percolation.[19,30]

4.1.1. Needles. Typical configurations generated by the model are shown in Figs. 2a–2c for $N = 2000$ needles for various values of p (1.0, 0.8,
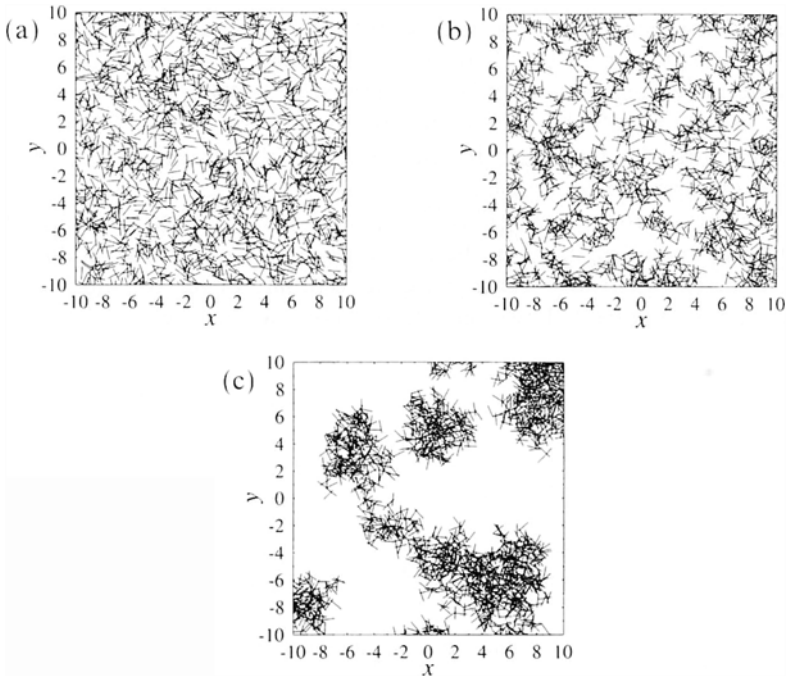

Fig. 2. Snapshot of a disordered network of $N = 2000$ deposited needles of length $\lambda = 1$ for (a) $p = 1.0$, (b) $p = 0.1$, and (c) $p = 0.001$.
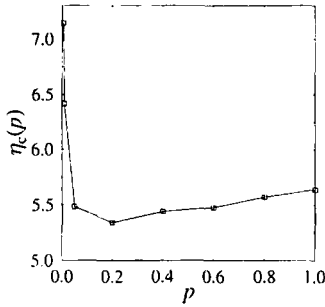
Fig. 3.   The critical percolation threshold $\eta_c(p)$ vs. p for a network of needles of length $\lambda = 1$ extrapolated to $L \to \infty$. The error bars are of the size of the points.

0.6, 0.4, 0.2, 0.05, 0.01, 0.005, and 0.001). The existence of well-defined clusters in the network for the smallest value of $p = 0.001$ is clearly visible. Employing the MCRG procedure for 1000 ensembles and for system sizes $L = 6$, 20, 30, 40, 60 for $0.2 \leqslant p \leqslant 1.0$ and $L = 6$, 20, 40, 60 for $0.005 \leqslant p \leqslant 0.05$, we obtain the values for $\eta_c(p)$ as displayed in Fig. 3. The curve displays interesting behavior in the two limits $p \to 0$ and $p \to 1$. The expected divergence of $\eta_c(p)$ in the limit $p \to 0$ is clearly visible, although for smallest p our results here and below are only qualitative due to strongly increasing finite-size effects. Moreover, $\eta_c(p)$ approaches the limit $p \to 1$ approximately linearly with a minimum at $p \approx 0.2$. These results together with the minimum in the curve visible around $p \approx 0.2$ will be further discussed in Section 4.2.

Our best estimate for $\eta_c(1) = 5.64 \pm 0.02$ agrees rather well with other numerical studies reported in the literature for the uniformly random case (see, e.g., ref. 23). It also agrees with the estimate of ref. 16, which gives a value of 5.61. Figure 4 shows the effective correlation length exponent $v(p)$
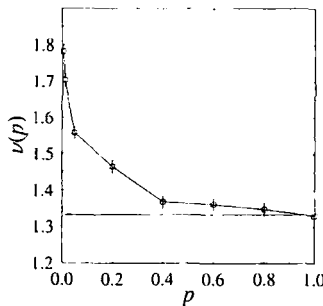

Fig. 4.   Correlation length exponent $v(p)$ vs. p for needles of length $\lambda = 1$. In this and the following figures for $v(p)$ the horizontal line denotes the exact value $v = 4/3$.

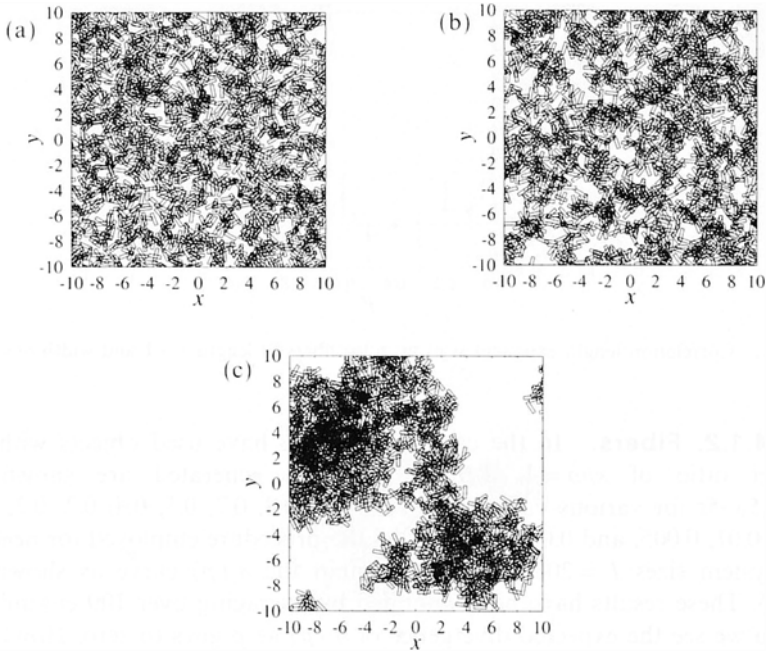Fig. 5. Snapshot of a disordered network of $N = 2000$ fibers of length $\lambda = 1$ and width $\omega = 1/4$. (a) $p = 1.0$, (b) $p = 0.1$, (c) $p = 0.001$.

as evaluated from the MCRG procedure. We note that $v(p)$ is consistent with $v = 4/3$ in the limit $p \rightarrow 1$. However, for $p \rightarrow 0$ the effective v increases. In Section 5 we show that this is due to increasing range of spatial correlations in the case where individual clusters become large. This induces strong crossover effects toward long-range correlated percolation type of behavior.[33]
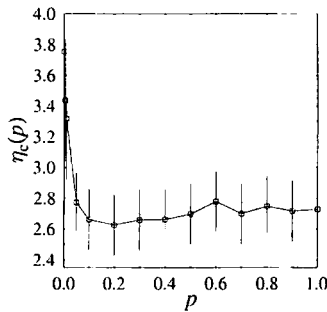

Fig. 6. The critical percolatuion threshold $\eta_c(p)$ vs. p for a network of fibers of length $\lambda = 1$ and width $\omega = 1/4$ extrapolated to $L \rightarrow \infty$. See text for details.
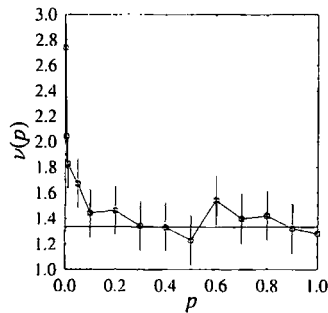
Fig. 7. Correlation length exponent $v(p)$ vs. p for fibers of length $\lambda = 1$ and width $\omega = 1/4$.

4.1.2. Fibers. In the case of fibers we have used objects with an aspect ratio of $\lambda/\omega = 4$. Typical networks generated are shown in Figs. 5a–5c for various values of p (1.0, 0.9, 0.8, 0.7, 0.5, 0.4, 0.3, 0.2, 0.1, 0.05, 0.01, 0.005, and 0.001). Following the procedure employed for needles for system sizes $L = 20$, 40, 80, we obtain the $\eta_c(p)$ curve as shown in Fig. 6. These results have been obtained by averaging over 100 ensembles. Again we see the expected divergence of $\eta_c(p)$ as p goes to zero. However, in the other limit $p \to 1$, $\eta_c(p)$ is almost constant within the error bars. Our best estimate for the $p = 1$ limit is $\eta_c(1) = 2.73 \pm 0.2$. To our knowledge, there are no other numrical studies of $\eta_c(1)$ for the present aspect ratio. However, $\eta_c(1)$ can be approximately determined by using the excluded-volume arguments of ref. 16, where $\eta_c(1)\langle A \rangle = \text{const} \approx 3.57$, and the excluded volume $\langle A \rangle = 1.379$.[11] This gives results within about 10% agreement with our numerical data. Finally, the correlation length exponent $v(p)$ is shown in Fig. 7. Again, as $p \to 1$, $v(p)$ is consistent with $v = 4/3$. Moreover, the effective $v(p)$ again increases as $p \to 0$.

4.1.3. Disks. For completeness we have also studied the case of isotropic disks. Typical networks of $N = 1000$ disks of radius $r_d = 0.5$ for various values of p (1.0, 0.9, 0.8, 0.7, 0.6, 0.5, 0.45, 0.4, 0.35, 0.3, 0.25, 0.2, 0.15, 0.1, 0.05, 0.02, 0.01, 0.005, and 0.001) are shown in Figs. 8a–8c. Following the procedure employed for needles for system sizes $L = 4$, 24, 32, 44, 64 and averaging over 800 ensembles for disks of radius $r_d = 1$, we obtain the $\eta_c(p)$ curve as shown in Fig. 9.[12] Again, $\eta_c(p)$ diverges as $p \to 0$.

---

[11] The excluded volume $\langle A \rangle$ can be evaluated from Eq. (19) of ref. 16 by using the present fiber dimensions and setting $\theta_\mu = \pi/2$.

[12] In the particular case of disks the spanning probabilities were obtained by fixing one direction and searching for the percolating cluster in that direction only.
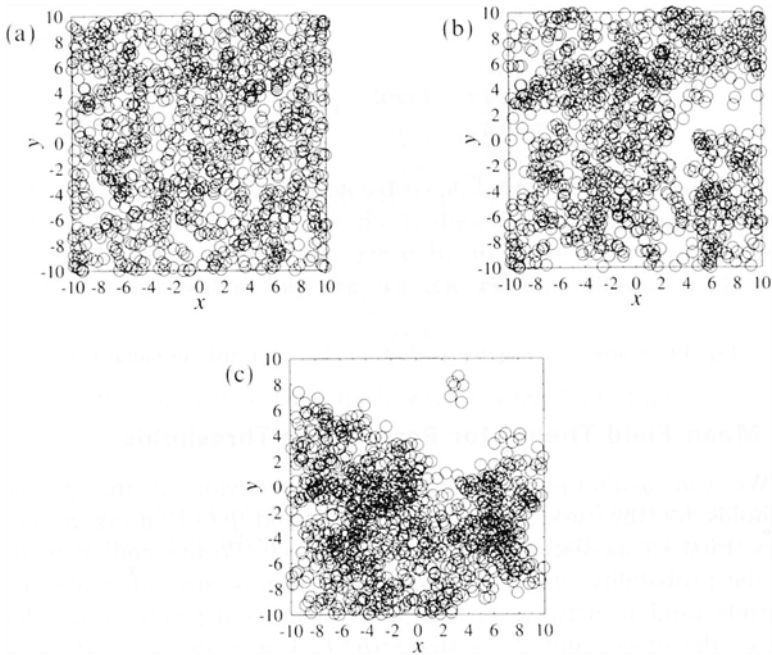
Fig. 8. Snapshot of a network of $N = 1000$ disks of radius $r_d = 0.5$ in a system of size $L = 20$. (a) $p = 1.0$, (b) $p = 0.1$, (c) $p = 0.001$.

However, for about $p > 0.3$, $\eta_c(p) \approx \text{const}$ within the error bars. We note that our best estimate for $\eta_c(1) = 0.374 \pm 0.016$ agrees within the errors with other numerical studies reported in the literature (see, e.g., ref. 21). The correlation length exponent $\nu(p)$ is shown in Fig. 10. Again, as $p \to 1$, $\nu(p)$ is consistent with $\nu = 4/3$. Also, the effective $\nu(p)$ increases as $p \to 0$.
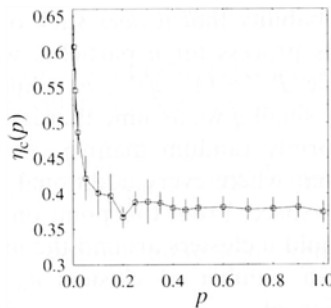

Fig. 9. The critical percolation threshold $\eta_c(p)$ vs. p for a network of disks of radius $r_d = 1$ extrapolated to $L \to \infty$.
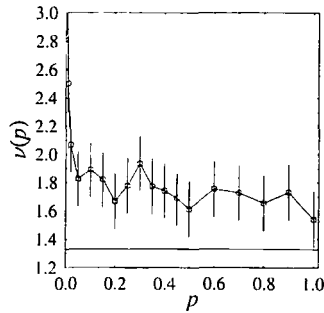
Fig. 10.   Correlation length exponent $\nu(p)$ vs. p for disks of radius $r_d = 1$.

4.2. Mean-Field Theory for Percolation Thresholds

We can *qualitatively* understand the behavior of the prcolation thresholds for the two limits where $p \to 0$ and $p \to 1$, using mean-field theory. First let us discuss the case where $p \to 0$. To this end let us define q as the probability of a given object intersecting any other object in a uniformly random network ($p = 1$). This quantity depends on the dimensions of the object and the system size L. For example, in the case of fibers[4]

$$q = \frac{2(\lambda + \omega)^2}{\pi L^2} + \frac{2\lambda\omega}{L^2} \tag{5}$$

For needles one can just set $\omega = 0$. Moreover, for disks a simple calculation gives $q = 9\pi r_d^2/L^2$.

Next consider the actual limit of $p \to 0$. Suppose we begin with an initially empty system and drop one object and then drop another. The probability that it sticks onto the 2D plane but *not* on the first one is $P_s^{(1)} = (1 - q)p$. The probability that it *does* stick on top of the first one is $Q_s^{(1)} = q$. Continuing this process for n particles, we find correspondingly that for the nth particle $P_s^{(n)} = (1 - q)^{n-1}p$, while $Q_s^{(n)} = 1 - (1 - q)^{n-1}$. Note that for sufficiently small q we assume that initially objectially objects tend to land in a uniformly random manner. For n greater than some $n = n_c$ there comes a point where every additional object will enounter as much occupied as empty space. From this point onward additional objects will essentially tend to build u clusters around the initial n_c seed objects. By this reasoning, the mean number of clusters n_c can be approximately obtained from the solution of

$$(1 - q)^{n_c - 1}p = 1(1 - q)^{n_c - 1} \tag{6}$$

which gives

$$n_c = 1 - \frac{\log(1 + p)}{\log(1 - q)} \tag{7}$$

We note that this equation is expcted to *underestimate* the true n_c due to the fact that due to clustering for $p < 1$, the effective excluded area of the objects will be smaller than that given by the bare q in Eq. (5). Let us assume that the growth of any one of the n_c clusters follows Eq. (1),

$$R_c = BN_c^{1/3} \tag{8}$$

where N_c is the number of particles in each cluster. Note that

$$N = n_c N_c \tag{9}$$

where N is the total number of objects in the network. On the average the system must percolate when the clusters begin to overlap, i.e., when

$$\sqrt{\frac{1}{\rho}} \approx 2R \tag{10}$$

where ρ is the density of clusters, $\rho = n_c/L^2$.

Substituting Eq. (7) into the expression for ρ and using Eq. (10), we obtain

$$2BN_c^{1/3} = L \left(1 - \frac{\log(1 + p)}{\log(1 - q)} \right)^{-1/2} \tag{11}$$

Using Eq. (9), we obtain

$$\eta_{c,L} = \frac{L}{8B^3} \left(1 - \frac{\log(1 + p)}{\log(1 - q)} \right)^{-1/2} \tag{12}$$

Equation (12) gives us the mean-field percolation threshold defined as $\eta_c \equiv \lim_{L \to \infty} \eta_{c,L}$. In particular, for the case of fibers we obtain

$$\eta_c = \sqrt{\frac{(\lambda + \omega)^2 + \lambda\omega\pi}{32\pi B^6}} \log^{-1/2}(1 + p) \tag{13}$$

This result is expected to become more and more accurate in the limit $p \to 0$, where it becomes

$$\eta_c = \sqrt{\frac{(\lambda + \omega)^2 + \lambda\omega\pi}{32\pi B^6}} \sqrt{\frac{1}{p}} \tag{14}$$

The result that $\eta_c \propto \sqrt{1/p}$ has also been obtained in a somwhat different manner in ref. 28, in accordance with our results. This universal inverse-square-root divergence on p is in qualitative agreement with the numrical data presented in Figs. 3, 6, and 9. However, due to the numrical difficulties in determining η_c accurately in this region, we have not been able to quantitatively verify Eq. (14). It is interesting to note that in the small-p limit, where percolation occurs through the growth of well-defined individual clusters, our model is somwhat similar to the cooperative lattice filling model, where cluster growth leads to percolation.[36] However, in this case there is no divergence of η_c, since overlap is not allowed.

Next we consider the other limit of $p \to 1$. Let us again start with a purely uniformly random case ($p = 1$) at its percolation threshold. The probability of any two particles intersecting is given by q as before. Take an arbitrary particle from the network of N particles. The probability $P_s^{(N)}$ is now given by

$$P_s^{(N)} = (1 - q)^{N-1} \tag{15}$$

Therefore, the number of nonintersecting objects will be, on the average,

$$N_s = P_s^{(N)} N \tag{16}$$

The main *qualitative* idea in the derivation here is the following. The effect of $p < 1$ is to reduce the number of nonintersecting objects due to clustering, but the backbone of the percolation cluster itself can be assumed to stay constant for p not too small. This already implies that the percolation threshold decreases as p decreases.

Let us next quantify this argument. Assume that the number of single particles removed that do not belong to the percolation cluster is given by

$$N_r = (1 - p) N_s \tag{17}$$

Therefore, the number of particles left at the percolation threshold for such p can be written as

$$\begin{aligned} N(p) &= N(1) - (1 - p) N_s \\ &= N(1) - (1 - p) P_s^{(N)} N(1) \end{aligned} \tag{18}$$

where $N(1)$ is the total number of particles within the uniformly random reference system with $p = 1$. For the critical density we thus obtain

$$\begin{aligned} \eta_{c,L}(p) &= \eta_{c,L}(1) - P_s^{(N)} \eta_{c,L}(1) + p P_s^{(N)} \eta_{c,L}(1) \\ &\equiv Ap + B \end{aligned} \tag{19}$$

Therefore, we can conclude that $\eta_{c,L}(p)$ increases linearly with p. This is also visible in our numerical data for the critical densities, at least for needles and fibers. To examine the theory quantitatively, we can show that for the case of fibers, in the limit $L \to \infty$,

$$A = \eta_c(1) \exp \left[-\eta_c(1) \left(\frac{2(\lambda + \omega)^2}{\pi} + 2\lambda\omega \right) \right] \qquad (20)$$

We have estimate A from the numerical data for needles and find that the numerical and theoretical values agree within about 50%.[13] The theoretical slope for disks is about an order of magnitude smaller than for needles, and thus it is not surprising that it is not discernible in our data of Fig. 9 within the error bars. Also, for the case of fibers the error bars are too large to see the slope.

The analytic derivations of this section can be used to explain the minimum in the $\eta_c(p)$ vs. p curves. Since in the limit $p \to 0$, $\eta_c(p)$ must diverge, whereas for p slightly below unity $\eta_c(p)$ must linearly decrease, it follows that a minimum must exist for some $0 < p < 1$. Physically, the existence of this minimum can be explained by a competition between two mechanisms in the model. First, single-cluster growth that dominates for small p is rather an inefficient way of forming the percolating cluster. On the other hand, uniform random filling of the lattice is inefficient, too, since there are many particles that do not belong to the percolating cluster. Thus, there is an "optimum" way of forming the cluster at some intermdiate value of p, where the critical density is minimal.

5. PAIR DISTRIBUTION AND THE TWO-POINT MASS DENSITY CORRELATION FUNCTION

In this section we begin by writing down a general expression for the two-point mass density correlation function for a random network of objects in which there is some effective particle–particle interaction. We then generalize this expression for the case of fiber networks. This expression involves the pair distribution function for the centers of the objects. This function has previously been derived exactly for the case of a uniformly random network of objects.[4,35] We generalize this derivation for

---

[13] To verify the argument that for p slightly less than unity the dominant effect is the removal of single needles from the network, we also calculated numerically the cluster size distributions. Since also clusters of two or more needles are removed, the analytic theory underestimates the slope of the curve for $p < 1$.

our model and compare the results with numerical simulations. We also examine in detail the form of the two-point mass density correlation function for the model.

5.1. A General Expression for the Two-Point Mass Density Correltion Function

The two-point density correlation function is generally defined as[37]

$$G(r) = \lim_{A \to \infty} f^{-1} \left(\frac{|\hat{\rho}(k)|^2}{A} \right) \tag{21}$$

where f is the 2D Fourier transform operator, $\hat{\rho}(k)$ is the Fourier transform of the mass density distribution, and $A = L^2$ is the area. This distribution can be written as

$$\rho(\mathbf{x}) = \sum_{i=1}^{N} \mu(\mathbf{x}, \mathbf{x}_i, \theta_i) \tag{22}$$

where $\mu(\mathbf{x}, \mathbf{x}_i, \theta_i)$ is equal to σ over the surface of particle i which is loated at the point $\mathbf{x}_i$ with orientation θ_i, and zero outside of it. Here σ is the mass density of each particle. Writing $\hat{\rho}(k) = \int_A \rho(\mathbf{x}) \exp(-2\pi i k \cdot \mathbf{x})$ and substituting into Eq. (21), we obtain after some algebra te general expression[38]

$$\hat{n}(k) = \eta \langle |I(k)|^2 \rangle + \langle |I(k)| \rangle^2 \lim_{A \to \infty} \frac{N(N-1)}{2A}$$

$$\times \left(\int_A \int_A \{ \exp[-2\pi i k \cdot (\mathbf{x}_i - \mathbf{x}_j)] \} \tilde{g}(|\mathbf{x}_i - \mathbf{x}_j|) \, d^2 x_i \, d^2 x_j \right) \tag{23}$$

where $\hat{n}(k) \equiv \lim_{A \to \infty} |\hat{\rho}(k)|^2 / (A\sigma^2)$ and η is the number density of the particles. This gives the correlation function as

$$G(r) = f^{-1}(\sigma^2 \hat{n}(k)) \tag{24}$$

In these equations $\langle |I(k)|^2 \rangle$ denotes the square of the Fourier transform of a single object averaged over all orientations. The second term in Eq. (23) contains the center–center pair distribution function $\tilde{g}(|\mathbf{x}_i - \mathbf{x}_j|)$,[38] which describes the effective interparticle interactions in the network. It gives the probability per unit area squared of particle center i occupying position $\mathbf{x}_i$ and that of another particle center j occupying position $\mathbf{x}_j$.

Making a change of variables and carrying out one of the integrals in Eq. (23) gives

$$\hat{n}(k) = \eta \langle |I(k)|^2 \rangle + \eta^2 \langle |I(k)| \rangle^2 \lim_{A \to \infty} \left(\int_0^{\sqrt{2}L} J_0(2\pi kr)[A\Omega(r)] \, dr \right) \quad (25)$$

where $J_0(x)$ is the Bessel function of order zero and we define $A\Omega(r) \equiv 2\pi r \tilde{g}(r)$. Equation (25) has two components. The first describes the self-correlation of single particles, while the second describes the cross-correlations, through the function $\Omega(r)$. The function Ω is defined as

$$\Omega(r) \, dr = \left\langle \frac{\# \text{ of pairs of centers in a shell } (r, r+dr)}{\text{total } \# \text{ of pairs of centers in system}} \right\rangle \quad (26)$$

where the averaging is over all configurations. The function $\Omega(r)$ in our final expression (25) contains the effects of particle interactions, while $I(k)$ contains the information about the geometry of the deposited objects. In the special case of fibers $I(k)$ has been derived exactly in ref. 37, giving

$$\langle |I(k)|^2 \rangle = (\lambda\omega)^2 \left(\frac{1}{2\pi} \int_0^{2\pi} \text{sinc}[\pi k\lambda \cos(t)] \, \text{sinc}[\pi k\omega \sin(t)] \, dt \right)^2 \quad (27)$$

and

$$|I(k)| \rangle^2 = (\lambda\omega)^2 \frac{1}{2\pi} \int_0^{2\pi} \text{sinc}^2[\pi k\lambda \cos(t)] \, \text{sinc}^2[\pi k\omega \sin(t)] \, dt \quad (28)$$

where $\text{sinc}(x) = \sin(x)/x$. In the previous studies the second term in Eq. (25) has been neglected for uniformly random fiber networks. However, for our model, where effective interactions arise for $p < 1$, the second term gives rise to nontrivial correlations that must be taken into account.

5.2. The Pair Distribution Function

An exact expression for $\Omega(r)$ in the case of uniformly random networks has previously been derived by Ghosh.[4,35] Below we will generalize this derivation to obtain an approximate formula for our model that is valid for small values of p. To begin with, let $\Delta N_{CM}(x_i)$ be the number of centers of masses within the area element $\Delta A(x_i)$ around the position vector x_i. The number of pairs included in two different area elements is

then given by the product $\Delta N_{\mathrm{CM}}(\mathbf{x}_i)\,\Delta N_{\mathrm{CM}}(\mathbf{x}_j)$. Further, the total number of pairs separated by vector $\mathbf{x}$ in a given configuration is

$$\sum_{\mathbf{x}_0} \Delta N_{\mathrm{CM}}(\mathbf{x}_0)\,\Delta N_{\mathrm{CM}}(\mathbf{x}_0+\mathbf{x}) \tag{29}$$

Dividing this by $N(N-1)/2$, we obtain the probability to find of centers of mass separated by the vector $\mathbf{x}$ in a given configuration. Multiplying and dividing by area elements yields

$$\Omega(r)\,dr = \frac{2}{N(N-1)} \left\langle \sum_{\mathbf{x}_0} \frac{\Delta N_{\mathrm{CM}}(\mathbf{x}_0)}{\Delta A(\mathbf{x}_0)} \frac{\Delta N_{\mathrm{CM}}(\mathbf{x}_0+\mathbf{x})}{\Delta A(\mathbf{x}_0+\mathbf{x})} \Delta A(\mathbf{x}_0)\,\Delta(\mathbf{x}_0+\mathbf{x}) \right\rangle \tag{30}$$

where we have assumed that the system is isotropic and thus Ω depends on $r \equiv |\mathbf{x}|$ only. The brackets denote configuration averaging. Taking the continuum limit where $\eta_{\mathrm{CM}} = \lim_{\Delta A \to 0}(\Delta N_{\mathrm{CM}}/\Delta A)$, we obtain

$$\Omega(r)\,dr = \frac{2}{N(N-1)} \left\langle \int_A d^2 x_0\, \eta_{\mathrm{CM}}(\mathbf{x}_0)\,\eta_{\mathrm{CM}}(\mathbf{x}_0+\mathbf{x})\,\Delta A(\mathbf{x}_0+\mathbf{x}) \right\rangle \tag{31}$$

Hence,

$$\Omega(r)\,dr = \frac{2}{N(N-1)} \int_A d^2 x_0\, G_{\mathrm{CM}}(r_0, r)\,\Delta A(r_0+r) \tag{32}$$

where

$$G_{\mathrm{CM}}(r_0, r) \equiv \langle \eta_{\mathrm{CM}}(\mathbf{x}_0)\,\eta_{\mathrm{CM}}(\mathbf{x}_0+\mathbf{x}) \rangle \tag{33}$$

It is easy to see that for a uniformly random set of points with translational invariance $G_{\mathrm{CM}}(r) = N(N-1)/(2A^2) = \mathrm{const}$ (no double counting of pairs), which leads to $A\Omega(r) = \Omega_h(r, L)$, with Ω_h being the previously derived exact pair distribution function for a uniform random network.[4,35] For large system size $(A \to \infty)$, $A\Omega(r) \to 2\pi r$. When this is substituted into Eq. (25) a constant term arises in the correlation function since there are no particle–particle interactions in this special case.

In the case of $p < 1$, where clustering occurs in the model, the pair distribution function $\Omega(r)$ gives rise to nontrivial correlations. In this case $\Omega(r)$ can still be derived approximately using mean-field arguments. A straightforward but lengthy calculation gives the result (see the Appendix for details)

$$\Omega(r) = \omega_1(N, p)\,g(r) + \omega_2(N, p)\,\Omega_h(r, L) \tag{34}$$

where

$$g(r) = \begin{cases} (30r/42R^5)(3r^3 - 6Rr^2 + 4R^3) & \text{for} \quad 0 \leqslant r \leqslant R \\ (30r/42R^5)(2R - r)^3 & \text{for} \quad R \leqslant r \leqslant 2R \\ 0 & \text{for} \quad 2R \leqslant r \end{cases} \qquad (35)$$

The coefficients are defined as $\omega_1(N, p) \equiv n_c N_c(N_c - 1)/[N(N-1)]$, where n_c and N_c are defined in Section 4, and $\omega_2(N, p) = 1 - \omega_1(N, p)$. In Eq. (34) $\Omega_h(r, L)$ denotes the pair distribution function for a uniformly random system that is given by[4,35]

$$\Omega_h(r, L) = \begin{cases} (4r/L^4)(\pi L^2/2 - 2rL + r^2/2) \\ \quad \text{for} \quad 0 \leqslant r \leqslant L \\ (4r/L^4)[L^2(\arcsin(L/r) - \arccos(L/r)) \\ \quad + 2L\sqrt{r^2 - L^2} - \tfrac{1}{2}(r^2 + 2L^2)] \\ \quad \text{for} \quad L \leqslant r \leqslant \sqrt{2} L \end{cases} \qquad (36)$$

As discussed in more detail in the Appendix, Eq. (34) is only approximately valid, although it does reduce to the exact limit $\Omega_h(r, L)$ for $p = 1$. It has been derived under the assumption that the deposited objects form clusters that grow independently following the scaling relations derived in Section 3. This approximation is best justified in the $p \to 0$ limit.

In Figs. 11a and 11b we illustrate several numerically obtained curves for $\Omega(r)$ for $p = 0.001$ and 0.01, respectively, in the case of fiber networks. There are two common features in the figures. First, for small values of N
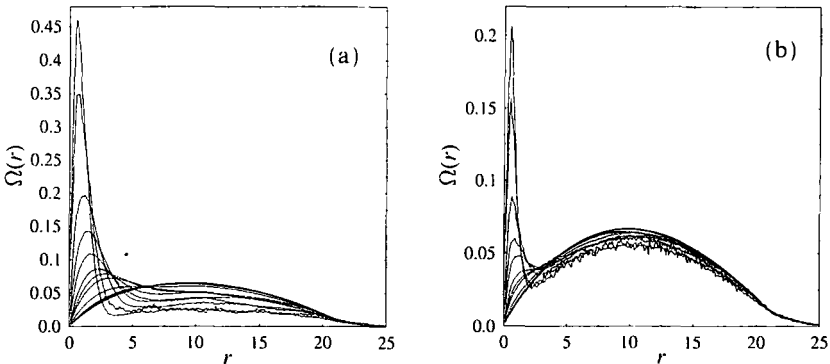

Fig. 11. Simulated pair distribution functions for fibres of length $\lambda = 1$ and width $\omega = 1/4$ for (a) $p = 0.001$ and (b) $p = 0.01$. The different curves correspond to $N = 15, 25, 75, 150, 250, 500, 750, 1000, 2000, 4000, 4500, 5000, 6000$ from top to bottom tracking the peak near the origin.

well below percolation $\Omega(r)$ develops a sharp peak near the origin. This peak is due to the cluster structure in the growing network. Moreover, its position is proportional to the average size of the clusters, as can be seen from Eq. (35). In the opposite limit of $N \to \infty$, $\Omega(r)$ approaches $\Omega_h(r, L)$ as expected, since the effect of p becomes gradually less important after the network has percolated. In the intermdiate regions a combination of the two effects is seen and a smooth transformation occurs between the two regimes. We note that when p increases, the height of the first peak decreases and its position shifts to smaller values of r, indicating that clusters become smaller.

To test quantitatively the accuracy of our analytic formula, we compared the numerically obtained function $\Omega(r)$ with our analytic result of Eq. (34). In Figs. 12a–12c we show the results of comparison for $p = 0.001$ with varying N. In evaluating the analytic formula, two quantities, namely
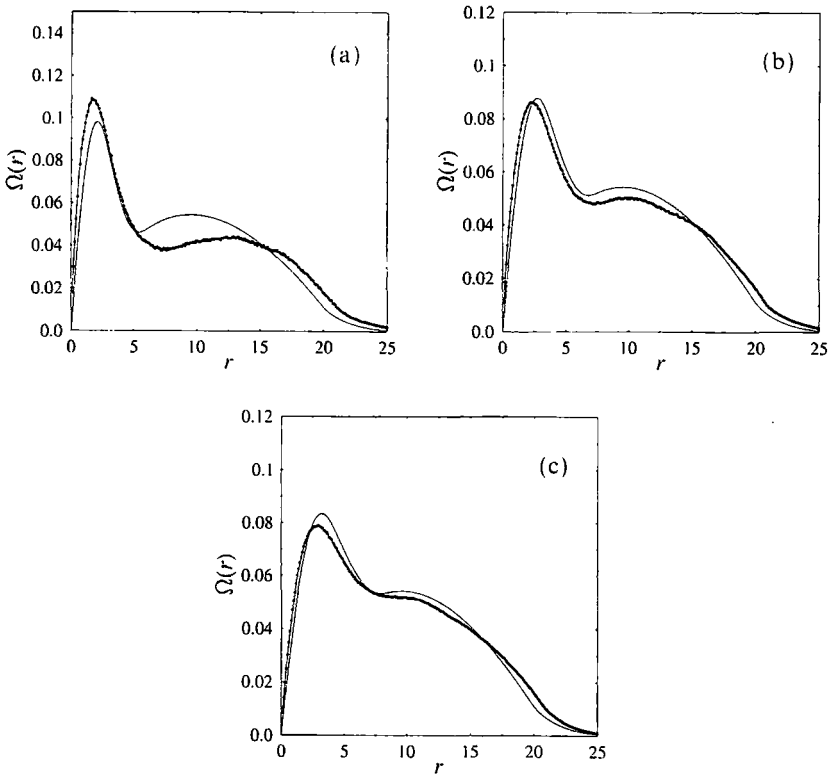

Fig. 12. Comparison between analytic (solid lines) and simulated (dotted lines) pair distribution functions for fibers of length $\lambda = 1$ and width $\omega = 1/4$ for $p = 0.001$ and $L = 20$. (a) $N = 250$, (b) $N = 500$, (c) $N = 750$. See text for details on this and the following figures.

the average cluster radius R and the number of clusters n_c, are needed. The latter can be evaluated from Eq. (7) for any p. However, since this equation underestimates the true number of clusters in the system, e.g., for $p = 0.001$ it gives $n_c \approx 1.2$, we have allowed n_c to be a fitting parameter. The quantity R, on the other hand, is fixed using the scaling relation $R = BN_c^{1/3}$, where N_c is the number of fibers in each cluster. This can be evaluated from the identity $N = n_c N_c$ (see Section 4.2). The only parameter left is the prefactor B, which we fix to be $B = 0.8$. This value has been extracted from numerical data for single-cluster growth. As seen in Figs. 12a–12c, setting $n_c = 4.5$ gives very good agreement between the theory and the simulations. This agreement also lends indirect support ro the inverse-square-root divergence of the percolation threshold on p derived in Section 4.2.

We should note that the derivation of the analytic formula is expected to be valid at most up to the point of percolation and for small values of p, since otherwise the whole picture of growing independent clusters breaks down. We have not carried out a systematic study of the range of validity of the theory for larger values of p, however.

5.3. The Two-Point Mass Density Correlation Function

Next we examine the two-point mass density correlation function for the model. In particular, we examine the case of fiber networks with an aspect ratio of $\lambda/\omega = 20/1$, which is rather close to the needle limit. We also discuss the effect of different object geometries on the correlation function. It can be obtained from our formalism by substituting the numerically evaluated $\Omega(r)$ into Eq. (25) and using Eq. (24). However, for simplicity we have calculated the correlation function directly from simulations on a lattice.[14] Defining $\tilde{G}(\mathbf{x}) \equiv \langle [m(\mathbf{x}') - \langle m \rangle][m(\mathbf{x}' + \mathbf{x}) - \langle m \rangle] \rangle$ to be the mss density–density *fluctuation* correlation function, we find that it form is well approximated by

$$\tilde{G}(r) \sim r^{-\alpha(N, p)} \qquad \text{for} \quad 0 < r < \Lambda(N, p) \qquad (37)$$

where Λ is an effective cutoff for the power-law form. In the case of $p = 1$ we obtain $\alpha \approx 1$ and $\Lambda \approx \lambda/2$. For lower values of p, however, $\tilde{G}(r)$ displays

---

[14] As a consistency check, we have explicitly verified that $\tilde{G}(r)$ as calculated from the analytic theory agrees with simulations of the lattice model for $p = 0.01$ and over a range of N for the choice of $L/\lambda/\omega = 400/20/1$. We solved our lattice model with periodic boundary conditions. For the system sizes used we found that the effect of the boundaries is not detectable.
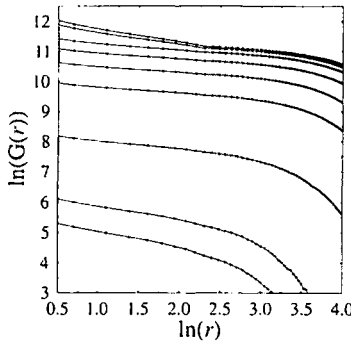
Fig. 13. A plot of $\ln(\tilde{G}(r))$ vs. $\ln(r)$ for fibers of length $\lambda = 20$ and width $\omega = 1$ for $p = 0.001$. From bottom to top, N increases with $N = 25$, 50, 300, 1500, 3000, 5000, 8000, 20000, 25000. The system size is $L = 400$.

interesting behavior, as illustrated in Fig. 13, where we show $\tilde{G}(r)$ on a logarithmic scale for $p = 0.001$. By examining the curves it can be inferred that $\alpha(N, p)$ goes through a minimum as N increases. Moreover, Λ attains a maximum where α is minimum.

Figure 14 shows the effective $\alpha(N, p)$ vs. N for the model for different values of p. The behaviour of α can be understood as a competition between individual fiber clusters and uniformly random fibers, which coexist for $0 < p < 1$. The correlation exponent approaches $\alpha = 1$ as $N \rightarrow \infty$ because in this limit the effect of p gradually becomes unimportant, as discussed in Section 5.2. On the other hand, the initial decrease of the effective $\alpha(N, p)$ for small values of N (as well as the increase of the range of the corresponding power-law regime) is due to the growth of essentially independent fiber clusters.
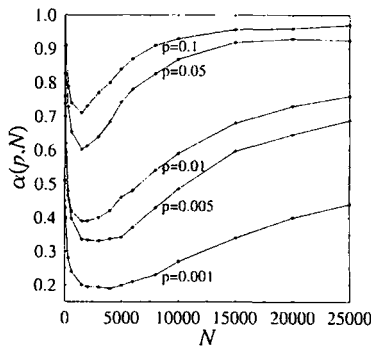

Fig. 14. A plot of the effective exponent $\alpha(N, p)$ vs. N for various p. The aspect ratio is $L/\lambda/\omega = 400/20/1$.
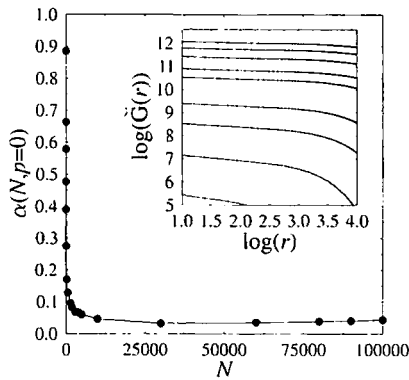
Fig. 15. A plot of $\alpha(N, p=0)$ vs. N for the special case where a single cluster grows with fibers of length $\lambda = 20$ and width $\omega = 1$ (see Fig. 1). Note the saturation to a constant $\alpha \approx 0.05$ after $N \approx 500$. The inset shows $\ln(\tilde{G}(r))$ vs. $\ln(r)$ for $N = 25$, 100, 300, 600, 1500, 2000, 4000, 5000, from bottom to top.

A better understanding of the low-N behavior of $\alpha(N, p)$, as well as the increase in the power-law regime, can be understood by considering the particular case of $p = 0$. In this limit only a single cluster emerges (see Fig. 1). We find that $\tilde{G}(r)$ as averaged over an ensemble of clusters of size N is also well approximated by a power-law form. Figure 15 shows $\alpha(N, p = 0)$ vs. N for this case. For the case of a large enough N (which is about 300–400 for the fibers here) α saturates to a fixed value of about 0.05. Moreover, we also find that the range of the power law is proportional to the radius of the cluster, with a constant of proportionality of about 0.7. We note that α reaches its saturated value approximately at the same value of N where the scaling laws of single cluster growth in Section 3 start to become valid.

We have also examined the correlation function for the fiber aspect ratio of $\lambda/\omega = 20/5$, which is away from the needle limit, and for isotropic disks. In the case of such fiber or disk networks we find that for values of N and p comparable to those of the needlelike case the correlation function is not as well approximated by a simple power-law behavior. However, as expected, the power-law behavior does eventually emerge for small enough values of p. The same conclusion also applies to single-cluster correlations where larger values of N are needed. Thus, we can conclude that the needle-like anisotropy enhances the emergence of power-law type of behavior in the system.

It is instructive to consider a random cluster network composed of a uniformly random distribution of fiber clusters, each of N fibers, in the needlelike limit. Following the method of Section 5, it is straightforward to

show that the correlation function $\tilde{G}(r)$ for such a network is given by Eq. (25), where $\langle |I|^2 \rangle$ now represents the square of the Fourier transform of a *single* cluster. In this case $\tilde{G}(r)$ is exactly proportional to the correlation function of single cluster discussed above, and the same power-law form emerges, with its range proportional to the cluster size. However, we note that, as discussed in ref. 29, even longer range power-law-type correlations for a network of fiber clusters can be obtained by assuming that there is an effective cluster–cluster interaction that gives rise to such correlations beyond the cluster size.

It is interesting to examine our results for the areal mss density fluctuation correlation function with recent measurement of this quantity for laboratory-made paper.[12] It has been shown that $\tilde{G}(r)$ for these paper sheets is well approximated by a power-law form whose exponent is independent of the mass density of paper and is $\alpha \approx 0.37$. Moreover, the range of this power law is rather short for high-basis-weight paper, i.e., of the order of the fiber length, whereas it becomes longer ranged for low-mass-density paper, extending even up to about 14 times the fiber length. It is interesting to note that the simple deposition model presented here can give similar values of α for values of N corresponding to real paper, by suitably adjusting p (see Fig. 14). However, the range of the power law in this case does not vary with mass density in the same way as in real paper. We can conclude from the results of this work that there are at least two possibilities of obtaining longer range correlations such as in low-mass-density paper. The first is that paper comprises small clusters between which there is an effective interaction giving rise to such correlations, as explained in ref. 29. The second is that paper can be described by deposition of larger, independent clusters whose internal correlations are of power-law type with $\alpha \approx 0.37$.[12] However, the true microscopic modeling of paper-making and unraveling of the reasons behind spatial correlations is a formidable theoretical problem.

6. SUMMARY AND CONCLUSIONS

In this paper we have studied growth, percolation, and correlation properties of disordered networks of fibers and other extended objects. In particular, we have introduced a deposition model that introduces an effective sticking of particles upon deposition. The key parameter of the model is the acceptance probability p, which describes the effective interactions between particles, thereby controlling the tendency to form clusters. This choice of rule is motivated by interactions that may be present in suspension during the formation phase of paper.

By varying p, the model interpolates between the growth of uniformly random networks ($p = 1$) and single-cluster growth ($p = 0$). We started by

studying the growth of single clusters and the form of the density profiles for such clusters. For both quantities analytic results have been derived and verified by numerical simulations. Following this, we examined the percolation threshold $\eta_c(p)$ of needles, fibers, and disks in detail by performing extensive numerical calculations as a function of p. In the limit $p = 1$ our results reduce to those previously obtained for needles and disks. In the case of rectangles, however, we were unable to make quantitative comparisons with the literature. Furthermore, our results were supplemented by mean-field arguments for the dependence of $\eta_c(p)$ in the limits $p \to 1$ and $p \to 0$.

An additional interesting feature of the model is the emergence of nontrivial spatial correlations for $p < 1$. We have examined these correlations by an approximate analytic calculation of the pair distribution function of a network of objects and have numerically examined this function for the case of fibers. Moreover, we have studied the two-point mass density fluctuation correlation function of the model and shown that on some cases it can be well approximated by a power-law type of form with a nontrivial exponent. This kind of power-law behavior is enhanced by increasing anisotropy of the deposited objects.

Finally, the results for the correlation function from the model are particularly interesting when contrasted with those obtained for mass density correlations in real paper sheets, where power-law type correlations arise in some cases. Further work on related, more complicated deposition models for fibers is in progress.

APPENDIX. THE PAIR DISTRIBUTION FUNCTION

In order to derive an expression for $\Omega(r)$, we need to know how to perform the ensemble average in Eq. (33). To derive an explicit form for $G_{\mathrm{CM}}(\mathbf{x}_0, \mathbf{x})$ we start with a general expression for the probability density $P[\rho]$ is a given fiber configuration, where ρ is the mass density:

$$P[\rho] = \int_A \prod_{k=1}^{N} d^2x_k \, B(\{\mathbf{x}_k, \theta_k\}) \, \delta\left[\rho(\mathbf{x}) - \sum_{s=1}^{N} \mu(\mathbf{x}, \mathbf{x}_s, \theta_s)\right] \quad \text{(A1)}$$

where μ has been defined in Eq. (22). The probability distribution for the centers of masses is readily obtained by replacing μ by a delta function.

To calculate correlation functions, the distribution function of the centers of masses B has to be provided. In what follows we will for simplicity drop the angular dependence from it. In the case we assume that p is so

small that during deposition single clusters emerge and start growing independently of each other, the distribution will factorize as

$$B(\{\mathbf{x}_k\}) = \prod_{m=1}^{n_c} B_{cl}(\{\mathbf{x}_s\}_m) \tag{A2}$$

where $\{\mathbf{x}_s\}_m$ denotes the set of the center-of-mass coordinates of the particles belonging to the mth cluster and n_c is the number of clusters. The assumption made here is that each particle must be uniquely assigned to one of the connected clusters in the network. The distribution of the particles inside each cluster B_{cl} is taken to be a completely symmetric function of all of its arguments. In Eq. (33) we will separate the different terms in the correlation function into two groups. First there are those terms that come from correlations between particles belonging to the same cluster (corresponding particle labels are i and j). The remaining contribution is collected from correlations between particles sitting in different clusters (labels I and J):

$$G_{\mathrm{CM}}(\mathbf{x}_0, \mathbf{x}) = \sum_{i,j} \int_A \prod_{k=1}^{N} d^2 x_k \, N(\{\mathbf{x}_k\}) \, \delta(\mathbf{x}_0 - \mathbf{x}_i) \, \delta(\mathbf{x}_0 + \mathbf{x} - \mathbf{x}_j) \tag{A3}$$

$$+ \sum_{I,J} \int_A \prod_{k=1}^{N} d^2 x_k \, B(\{\mathbf{x}_k\}) \, \delta(\mathbf{x}_0 - \mathbf{x}_I) \, \delta(\mathbf{x}_0 + \mathbf{x} - \mathbf{x}_J) \tag{A4}$$

Due to the indistinguishability of the particles, the first sum on the RHS of the previous equation can be replaced with a factor $\tilde{\omega}_1 \equiv n_c N_c (N_c - 1)/2$. Similarily, the second sum gives rise to a factor $\tilde{\omega}_2 \equiv N(N-1)/2 - n_c N_c(N_c - 1)/2$. Hence,

$$G_{\mathrm{CM}}(\mathbf{x}_0, \mathbf{x}) = \tilde{\omega}_1 \int_A \prod_p d^2 x_p \, B_{cl}(\{\mathbf{x}_p\}) \, \delta(\mathbf{x}_0 - \mathbf{x}_i) \, \delta(\mathbf{x}_0 + \mathbf{x} - \mathbf{x}_j) \tag{A5}$$

$$+ \tilde{\omega}_2 \int_A \prod_p d^2 x_p \, B_{cl}(\{\mathbf{x}_p\}) \, \delta(\mathbf{x}_0 - \mathbf{x}_I)$$

$$\times \int_A \prod_q d^2 x_q \, B_{cl}(\{\mathbf{x}_q\}) \, \delta(\mathbf{x}_0 + \mathbf{x} - \mathbf{x}_J) \tag{A.6}$$

$$\equiv \tilde{\omega}_1 B_{cl}^{(1)}(\mathbf{x}_0, \mathbf{x}_0 + \mathbf{x}) + \tilde{\omega}_2 B_{cl}^{(2)}(\mathbf{x}_0) \, B_{cl}^{(2)}(\mathbf{x}_0 + \mathbf{x}) \tag{A7}$$

In the equation above, particle coordinates $\{x_p\}$ belong to one of the n_c identical clusters ($\mathbf{x}_i, \mathbf{x}_j \in \{x_p\}$) and x_q belongs to another cluster ($\mathbf{x}_I \in \{x_p\}$ and $\mathbf{x}_J \in \{x_q\}$).

The quantity $B_{cl}(\{\mathbf{x}_p\})\prod_p d^2x_p$ gives the probability of finding the centers of the masses of the particles within one cluster at positions $\mathbf{w}_p$. Relative to the center of mass $\mathbf{x}_{cl}$ of the cluster these centers of masses cannot be scattered around the whole system at random positions, for the cluster is assumed to form a connected structure. From single-cluster growth theory we know that the mass density ρ a conelike function [given by Eq. (3)] with radius R. We assume that the number density η_{CM} of the centers of masses of particles is proportional to the mass density ρ in the cluster. The first term $B_{cl}^{(1)}(\mathbf{x}_0, \mathbf{x}_0 + \mathbf{x})$ is obtained by integrating out the positions of all the other centers of masses of particles but two, which are fixed at the positions $\mathbf{x}_0$ and $\mathbf{x}_0 + \mathbf{x}$. A nonzero contribution from the integrations will emerge only from those regions where the two fixed points are within a distance R from the center of mass $\mathbf{x}_{cl}$ of the cluster, i.e., when they belong to the cluster. Furthermore, we assume that the number of particles in the cluster is large enough so that $\mathbf{x}_{cl}$ is independent of the two points $\mathbf{x}_0$ and $\mathbf{x}_0 + \mathbf{x}$. Thus, we can write

$$B_{cl}^{(1)}(\mathbf{x}_0, \mathbf{x}_0 + \mathbf{x}) = C_1 \int_A d^2x_{cl}\, \rho(\mathbf{x}_0 - \mathbf{x}_{cl})\, \rho(\mathbf{x}_0 + \mathbf{x} - \mathbf{x}_{cl}) \tag{A8}$$

$$B_{cl}^{(2)}(\mathbf{x}_0) = C_2 \int_A d^2x_{cl}\, \rho(\mathbf{x}_0 - \mathbf{x}_{cl}) \tag{A9}$$

where C_1 and C_2 are normalization constants (B_{cl} is a probability density). The integration domain can be extended over the whole system since $\rho(r) = 0$ when $r > R$. Substitution of $G_{CM}(\mathbf{x}_0, \mathbf{x})$ into Eq. (32) yields

$$\Omega(r)\, dr = \omega_1\, g(r)\, dr + \omega_2 \Omega_h(r, L)\, dr \tag{A10}$$

where

$$\omega_1 \equiv \tilde{\omega}_1 \frac{2}{N(N-1)}, \qquad \omega_2 \equiv \tilde{\omega}_2 \frac{2}{N(N-1)}$$

and

$$g(r)\, dr = \int_A d^2x_0\, B_{cl}^{(1)}(\mathbf{x}_0, \mathbf{x}_0 + \mathbf{x})\, \Delta A(\mathbf{x}_0 + \mathbf{x}) \tag{A11}$$

$$= 2\pi r\, dr\, C_1 L^2 \int_K d^2x_0\, \rho(\mathbf{x}_0 - \mathbf{x}_{cl})\, \rho(\mathbf{x}_0 + \mathbf{x} - \mathbf{x}_{cl}) \tag{A12}$$

$$\Omega_h(r, L)\, dr = C_2^2 \int_A d^2x_0 \int_A d^2x_{cl}\, \rho(\mathbf{x}_0 - \mathbf{x}_{cl})$$

$$\times \int_A d^2x'_{cl}\, \rho(\mathbf{x}_0 + \mathbf{x} - \mathbf{x}'_{cl})\, \Delta A(\mathbf{x}_0 + \mathbf{x}) \qquad (A13)$$

$$= \int_A d^2x_0\, \Delta A(\mathbf{x}_0 + \mathbf{x}) \qquad (A14)$$

where the integration domain K in Eq. (A12) is given by $|\mathbf{x}_0 - \mathbf{x}_{cl}| \leqslant R$ and $|\mathbf{x}_0 + \mathbf{x} - \mathbf{x}_{cl}| \leqslant R$, which is the region where there is a nonzero contribution to $g(r)$. This means that we can make the transformation of variables $\mathbf{u} = \mathbf{x}_0 - \mathbf{x}_{cl}$, $2\mathbf{v} = \mathbf{x}_0 + \mathbf{x}_{cl}$, and thus the final result only depends on $r \equiv |\mathbf{x}|$.

In $d = 2$, $C_1 = (L\pi R^2 a/3)^{-2}$ and $C_2 = (L^2\pi R^2 a/3)^{-1}$ with $a \equiv \rho(0, N)$. The density ρ is given in Eq. (3). Substituting it into Eq. (A12) and setting $\Delta A(\mathbf{x}_0 + \mathbf{x}) = 2\pi r\, dr$, which is true within each cluster, yields $g(r)$. To get some insight into how g behaves, we will use one-dimensional density profiles instead of two-dimensional ones. However, we do not replace $\Delta A(\mathbf{x}_0 + \mathbf{x})$ with its one-dimensional counterpart, $\Delta A(\mathbf{x}_0 + \mathbf{x}) = 2\, dr$, since we want to satisfy the relation $g(0) = 0$, which is true in $d = 2$. In this case the normalization constant C_1 is given by $C_1 = 15/(7L^2\pi R^3 a^2)$. This gives as the final result Eq. (35).

Finally, we would like to note that in Eq. (A14), $\Delta A(\mathbf{x}_0 + \mathbf{x})$ imposes a cutoff at the edges of the system. This area element can be written in the form

$$\int_A d^2x_0\, \Delta A(\mathbf{x}_0 + \mathbf{x}) = r\, dr \int_A d^2x_0\, u(\mathbf{x}_0, \mathbf{x}) \qquad (A15)$$

where $\beta(\mathbf{x}_0, \mathbf{x})$ is the maximum angle swept by a vector of length $r = |\mathbf{x}|$ rotated around a fixed position $\mathbf{x}_0$, with the constraint that the vector must lie inside the system. This can be used in deriving the pair distribution function of a uniformly random system Ω_h, as given by Eq. (36).

ACKNOWLEDGMENTS

REFERENCES

1. J. W. Evans, *Rev. Mod. Phys.* **65**:1281 (1993).
2. V. Privman, In *Annual Reviews in Computational Physics*, Vol. 3, D. Stauffer, ed. (World Scientific, Singapore, 1995).

3. G. Y. Onoda and E. G. Liniger, *Phys. Rev. A* **33**:715 (1986); A. Schmit, R. Varoqui, S. Uniyal, J. L. Brash, and C. Pusiner, *J. Colloid Interface Sci.* **92**:25 (1983); J. Feder and I. Giaever, *J. Colloid Interface Sci.* **78**:144 (1980).
4. M. Deng and C. T. J. Dodson, *Paper: An Engineered Stochastic Structure* (Tappi Press, 1994).
5. K. J. Niskanen and M. J. Alava, *Phys. Rev. Lett.* **73**:3475 (1994).
6. P. Nielaba and V. Privman, *Phys. Rev. E* **51**:2022 (1995).
7. N. Ryde, H. Kihira, and E. Matijevic, *J. Colloid Interface Sci.* **151**:421 (1992).
8. A.-L. Barabasi and H. E. Stanley, *Fractal Concepts in Surface Growth* (Cambridge University Press, Cambridge, 1995).
9. C. A. Murray and D. G. Grier, *Am. Sci.* **83**:238 (1995).
10. M. L. Kurnaz and J. V. Maher, *Phys. Rev. E* **53**:978 (1996).
11. S. Schwarzer, *Phys. Rev. E* **52**:6461 (1995).
12. N. Provatas, M. J. Alava, and T. Ala-Nissila, *Phys. Rev. E* **54** (1996). N. Provatas, M. J. Alava, and T. Ala-Nissila, Unpublished (1996).
13. G. E. Pike and C. H. Seager, *Phys. Rev. B* **10**:1421 (1974).
14. I. Balberg and N. Binenbaum, *Phys. Rev. B* **28**:3799 (1983).
15. P. C. Robinson, *J. Phys. A* **16**:605 (1983).
16. I. Balberg, C. H. Anderson, S. Alexander, and N. Wagner, *Phys. Rev. B* **30**:3933 (1984).
17. P. C. Robinson, *J. Phys. A* **17**:2823 (1984).
18. A. L. R. Bug, S. A. Safran, and G. S. Grest, *Phys. Rev. Lett.* **55**:1896 (1985).
19. I. Balberg, *Phil. Mag. B* **56**:991 (1987).
20. D. Laría and F. Vericat, *Phys. Rev. B* **40**:353 (1989).
21. S. B. Lee and S. Torquato, *Phys. Rev. A* **41**:5338 (1990).
22. U. Alon, I. Balberg, and A. Drory, *Phys. Rev. Lett.* **66**:2879 (1991).
23. C. Vanneste, A. Gilabert, and D. Sornette, *Phys. Lett. A* **155**:174 (1991).
24. A. Drory, I. Balberg, and B. Berkowitz, *Phys. Rev. E* **49**:949 (1994).
25. H. S. Choi, J. Talbot, G. Tarjus, and P. Viot, *Phys. Rev. E* **51**:1353 (1995).
26. M. D. Rintoul and S. Torquato, *Phys. Rev. E* **52**:2635 (1995).
27. W. J. Boudville and T. C. McGill, *Phys. Rev. B* **39**:369 (1980).
28. J. Aström, Pro Gradu avhandling, Abo Akademi, Unpublished (1989).
29. N. Provatas, T. Ala-Nissila, and M. J. Alava, *Phys. Rev. Lett.* **75**:3556 (1995).
30. D. Stauffer and A. Aharony, *Introduction to Percolation Theory* (Taylor and Francis, London, 1994).
31. J. Hoshen and R. Kopelman, *Phys. Rev. B* **14**:3438 (1976).
32. P. J. Reynolds, H. E. Stanley, and W. Klein, *Phys. Rev. B* **21**:1223 (1980).
33. A. Weinrib, *Phys. Rev. B* **29**:387 (1984).
34. O. J. Kallmes and H. Corte, *Tappi J.* **43**:737 (1960).
35. B. Ghosh, *Calcutta Math. Soc.* **43**(1):17 (1951).
36. D. E. Sanders and J. W. Evans, *Phys. Rev. A* **38**:4186 (1988).
37. L. Haugland, B. Norman, and D. Wahren, Svensk Papperstidning no. 10, 362 (1974).
38. J.-P. Hansen and I. R. McDonald, *Theory of Simple Liquids* (Academic Press, New York, 1986).
39. R. J. Kerekes and C. J. Shell, *J. Pulp Paper Sci.* **18**:J32 (1992).